Journal of Nuclear Materials 401 (2010) 91–97

Contents lists available at ScienceDirect

Journal of Nuclear Materials

journal homepage: www.elsevier.com/locate/jnucmat

Incoherent Quasielastic Neutron Scattering study of hydrogen diffusion in thorium–zirconium hydrides

Kurt A. Terrani [a,*], Eugene Mamontov [b], Mehdi Balooch [a], Donald R. Olander [a]

[a] Department of Nuclear Engineering, University of California, 4155 Etcheverry Hall, M.C. 1730, Berkeley, CA 94720-1730, United States
[b] Spallation Neutron Source, Oak Ridge National Laboratory, P.O. Box 2008 MS-6473, Oak Ridge, TN 37831-6473, United States

ARTICLE INFO

Article history:
Received 21 August 2009
Accepted 11 April 2010

ABSTRACT

Monophase thorium–zirconium hydrides ($ThZr_2H_x$) have been fabricated starting from a metallic alloy and the hydrogen stoichiometry determined by X-ray diffraction. Incoherent Quasielastic Neutron Scattering (IQNS) on the hydrides was conducted over the temperature range 650–750 K at the Backscattering Silicon Spectrometer (BASIS) at the Spallation Neutron Source (SNS) at ORNL. The isotropic Chudley–Elliott model was utilized to analyze the quasielastic linewidth broadening data as function of momentum transfer. The diffusion coefficient and average jump distance of hydrogen atoms in $ThZr_2H_{5.6}$ and $ThZr_2H_{6.2}$ were extracted from the measurements.

1. Introduction

The thorium–zirconium alloy (Th:Zr = 1:2) reacts with hydrogen gas to form a monophase hydride with the hydrogen stoichiometry variable from 4 to 7 [1]. Hydrides with high hydrogen-to-metal (H/M) ratios are stable at temperatures typical of nuclear-reactor fuel operation. The presence of hydrogen in the fuel has neutronic advantages over oxide fuel, including thermally-induced hydrogen up-scattering of neutrons which provides a negative fuel reactivity coefficient at high temperatures. Fuels utilizing thorium–zirconium hydrides as one of their constituents have been fabricated, irradiated, and characterized [2,3].

Normal reactor operation results in higher temperatures at the centerline of the fuel pellet than at the surface. This temperature gradient causes hydrogen redistribution by thermal diffusion (Soret effect) [4]. Hydrogen accumulation at the pellet periphery and the corresponding depletion at the center generates stress gradients due to expansion or contraction of the lattice as the H/M ratio changes. For the case of a reactivity insertion accident (RIA) or loss of coolant or flow throughout the core, the fuel temperature could increase significantly, forcing hydrogen redistribution or release from the fuel [5]. Therefore the diffusion coefficient of hydrogen in $ThZr_2$ hydrides is an important parameter that needs to be measured in order to predict the kinetics of the redistribution process and to model the fuel behavior under steady-state or transient-power conditions. Determination of the hydrogen diffusion coefficient in thorium–zirconium hydrides, through the means of IQNS, is the subject of this paper.

2. Thorium–zirconium hydride ($ThZr_2H_x$)

The crystal structure of $ThZr_2H_x$ is cubic with a $Fd\bar{3}m$ space group. Bartscher et al. [1] have measured the lattice parameter of $ThZr_2$ hydrides and deuterides using X-ray diffraction and report the lattice parameter of the cubic unit cell as function of hydrogen or deuterium to metal ratio at room temperature (Fig. 1). However, the extent of uncertainty in the hydrogen and deuterium content of each compound is not reported, introducing further errors into the Vegards law model that is fitted through this data. Neutron powder diffraction experiments reveal that the hydrogen atoms are located in two different tetrahedral interstitial sites in the structure [6]. One is the 32e location, a site surrounded by one thorium and three zirconium atoms (four sites per formula), and the other is the 96g location, a site surrounded by two thorium and two zirconium atoms (12 sites per formula). The fractional occupancy of hydrogen in the 32e and 96g sites, in the range of stoichiometries of interest, is approximately 0.5 and 0.3, respectively. A schematic of the structure for this phase is presented in Fig. 2.

3. Material processing

Ternary $ThZr_2H_x$ compounds exist over a wide range of hydrogen stoichiometries. Compounds of higher hydrogen content are of particular interest for thermal nuclear reactor applications since these compositions provide good neutron moderation while retaining adequately low hydrogen overpressures (thermodynamic stability). Pressure–temperature-composition equilibrium information exists for the ternary compound [1], enabling the desired stoichiometry to be selectively processed through precise control of the temperature and hydrogen gas pressure during hydriding.

* Corresponding author. Tel.: +1 510 642 4077; fax: +1 510 643 9685.
E-mail address: terrani@berkeley.edu (K.A. Terrani).

0022-3115/$ - see front matter © 2010 Elsevier B.V. All rights reserved.
doi:10.1016/j.jnucmat.2010.04.003

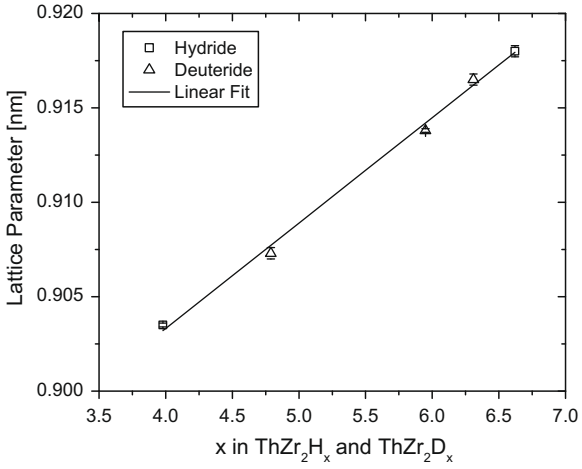

Fig. 1. Lattice parameter as function of hydrogen/deuterium-to-metal ratio in $ThZr_2H_x$ and $ThZr_2D_x$ [1].

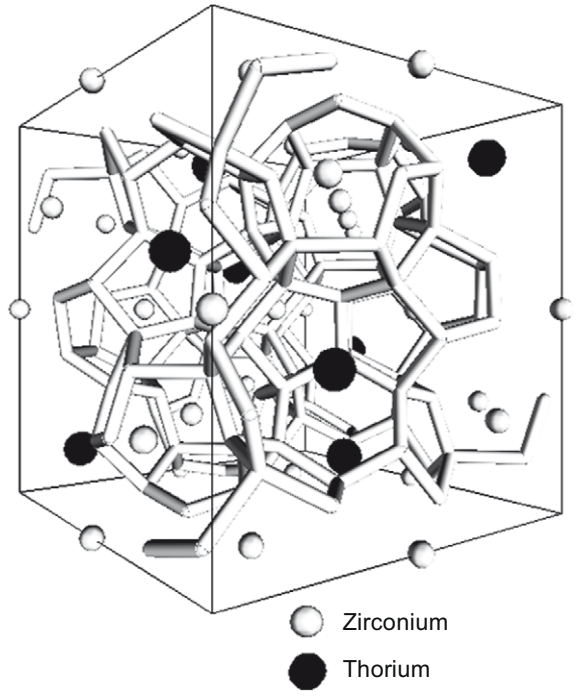

Fig. 2. Crystal structure of $ThZr_2H_x$ (space group: $Fd\bar{3}m$). The hydrogen network is depicted in the form of polyhedra around the zirconium and thorium atoms.

Initially a $ThZr_2$ alloy was prepared by the Materials Preparation Center at Ames Laboratory starting from high-purity feedstock (99.93 at.% Zr and 99.97 at.% Th). The elements were mixed to the desired ratio and electron-beam melted (with five remeltings) to form 15 g of the homogenous alloy. Examination of the Th–Zr binary phase diagram [7] implies that the melt initially solidifies into the BCC β-phase; a solid solution of thorium and zirconium. Upon cooling, if adequate time is given to reach equilibrium conditions, α-Th would start to precipitate at temperatures around 1173 K; while at temperatures below 923 K, all of the remaining β-phase would decompose into α-Th and α-Zr through a eutectoid reaction.

The microstructure of the electron-beam melted metal alloy was investigated using scanning electron microscopy in the backscattering mode in Fig. 3a. Scanning electron microscopy was performed on a FEI instrument model XL30-SFEG equipped with secondary and backscatter electron detectors and an EDAX Phoenix EDS (energy dispersive X-ray spectroscopy) system. The accelerating potential during operation was 20 kV. Contrast in the electron microscope image in the backscattering mode is a function of the difference between the average atomic number of the phases that are present. The microstructure of the metal alloy prior to hydriding, shown in Fig. 3a, is very fine; needle shape thorium grains (white phase) and spherical zirconium grains (black phase) have partially precipitated from the high temperature BCC solid solution (grey phase). EDS technique was also utilized to verify the composition of the overall alloy as shown in Fig. 4. Due to the very fine microstructure and lack of spatial resolution, each phase could

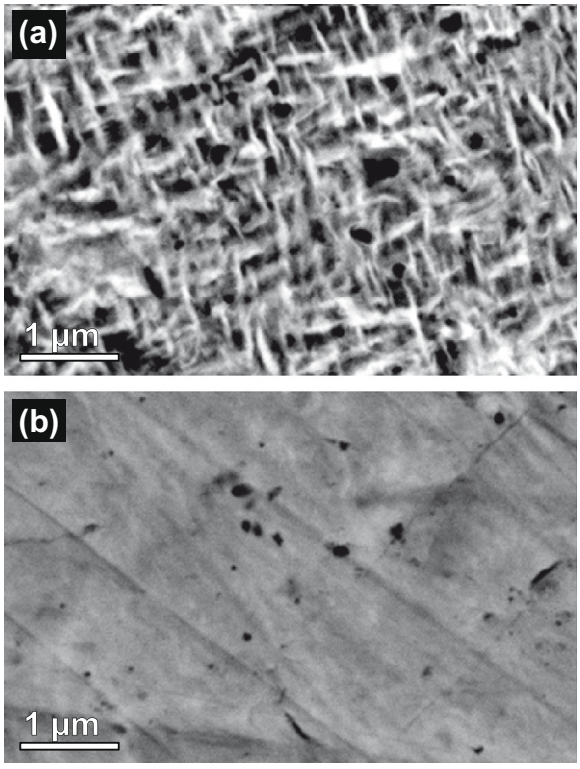

Fig. 3. Backscattered electron image of: (a) electron-beam melted $ThZr_2$ alloy (b) $ThZr_2H_{5.6}$.

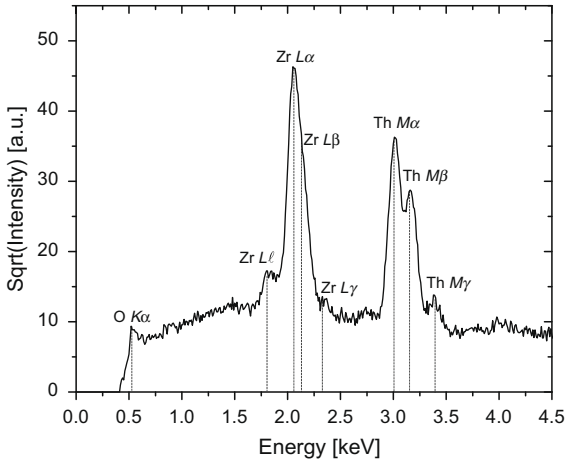

Fig. 4. Energy dispersive X-ray spectroscopy on electron-beam melted $ThZr_2$ alloy from the area shown in Fig. 3a.

not be examined separately. Meanwhile, the EDS results confirm that the metal alloy is free of impurities and solely consists of thorium and zirconium.

Thin disks of the metal alloy (~0.5 mm) were placed in a stainless steel vessel while the temperature and H_2 pressure were maintained constant for 30 min to achieve a uniform hydrogen concentration across the disk thickness. The hydrogen stoichiometry of the synthesized specimens was determined by X-ray diffractometry (XRD) with 80% confidence interval (see Table 1). This was done by matching the measured lattice parameter with what is previously reported based on X-ray diffraction experiments on hydrides and deuterides (Fig. 1). Hydride powders, mixed with lanthanum hexaboride (LaB_6 SRM660a) powder, were deposited on a low background silicon single-crystal sample holder using a slurry of powder mixture and ethanol to prepare the XRD samples. LaB_6 was employed as an internal standard during pattern refinement. A Phillips PANalytical X'Pert Pro instrument with a Cu Kα source was used to obtain high-resolution diffraction patterns. Results of the XRD experiment performed on $ThZr_2H_{5.6}$ mixed with LaB_6 confirm formation of a single phase hydride as well as the presence of some unknown Bragg peaks (Fig. 5). None of the following phases (accompanied by the associated space group), corresponding to any other hydrides or metallic alloys of thorium and/or zirconium, were detected in any significant amount in the diffraction patterns: δ-$ZrH_{1.6}$ ($Fm\bar{3}m$), ε-$ZrH_{1.8}$ ($I4/mmm$); ZrH ($P42/n$); ThH_2 ($I4/mmm$); Th_4H_{15} ($I\bar{4}3d$); Zr ($P6_3/mmc$); ThZr ($Im\bar{3}m$); Th ($Fm\bar{3}m$). For the X-ray diffraction experiment, the material is crushed into a very fine powder and exposed to air resulting in the possible formation of oxide products. The unknown Bragg peaks are therefore either due to foreign contamination or oxide products. The backscattering electron image of the $ThZr_2H_{5.6}$ hydride specimen in Fig. 3b also shows formation of a uniform monophase. Negligible extent of a second phase is also apparent in the form of black particles within the grey matrix (the black regions are not pits or wholes).

XRD and microscopy results confirm that the $ThZr_2H_x$ is the dominant phase that has formed after the hydriding and hydrogen is only present within this phase. The influence of the unknown phase on the results of the IQNS experiment can be disregarded for two reasons. First, the volume fraction of this phase is very negligible and the possible incoherent-neutron-scattering signal from this phase is very limited. Second and most importantly, the incoherent neutron scattering cross section for hydrogen is the second largest in the periodic table (10^5 times larger than that of oxygen), only behind gadolinium. Consequently, the incoherent-neutron-scattering signal measured in this experiment is dominated by the hydrogen in $ThZr_2H_x$ phase. For this same reason, the presence of thorium, zirconium, and aluminum in the metal hydride matrix is inconsequential to the measurement of hydrogen diffusion coefficient.

Table 1
Conditions for hydriding of 0.5 mm-thick alloy disks and the resulting lattice parameter and stoichiometry.

Temperature (°C)	Hydrogen pressure (MPa)	Lattice parameter (nm)	Hydrogen stoichiometry
700	0.15	0.9150	6.2 ± 0.1
825	0.12	0.9119	5.6 ± 0.1

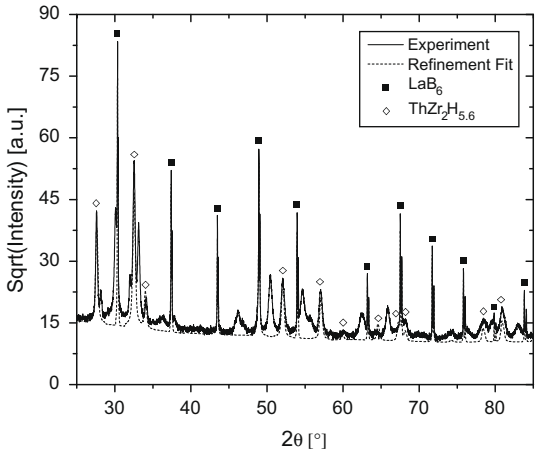

Fig. 5. Powder X-ray diffraction pattern for $ThZr_2H_{5.6}$ and LaB_6 standard along with Rietveld refinement fit.

4. Experimental details

A useful review of IQNS theory and experimental techniques is provided by Hempelmann [8] and can provide background information for the following sections. For this experiment an all aluminum sample holder was utilized consisting of two 2.75″ ConFlat (CF) flanges (Al-6061-T6), an aluminum gasket (Al-1060), and aluminum nuts and bolts (Al-2024-T4). Aluminum is ideal because it is almost entirely a coherent scatterer of neutrons. Utilization of the CF flange assembly guaranteed a leak-proof container under the high-vacuum conditions of the beam chamber (10^{-4} Pa). Due to the large hydrogen content of the material, multiple scattering at low angles is of concern for thick samples. The hydride pieces were crushed into fine powder and diluted with high-purity

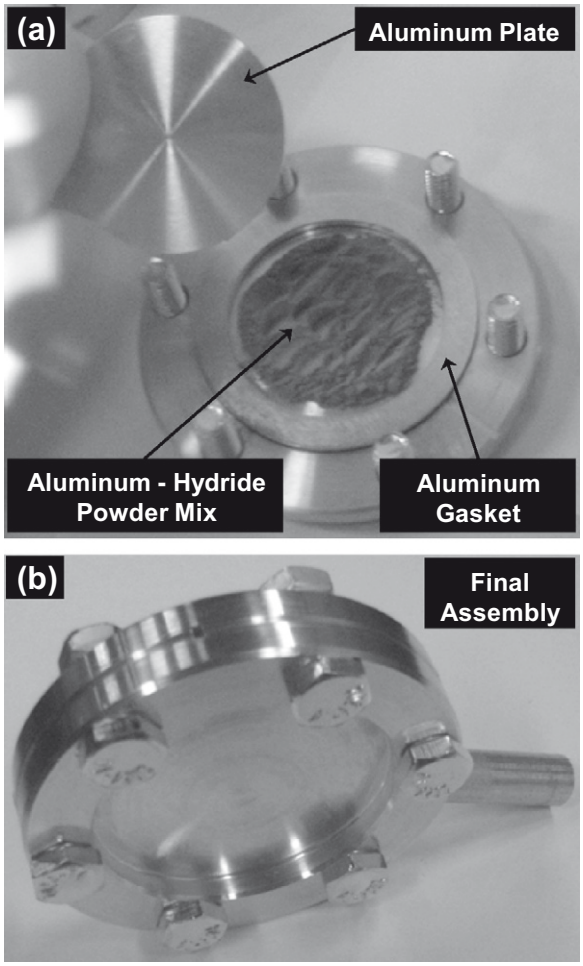

Fig. 6. (a) Sample holder during assembly (b) and its final configuration.

(99.99%) aluminum powder (10 vol% $ThZr_2H_x$ – 90 vol% Al). The powder mixture was spread thin into a 0.5 mm thick layer held tightly between the two flanges and an aluminum plate (Al-6061-T6) with thickness of 1.94 mm (the plate was used to fill up the entire available volume). The central region (at the exterior) of the CF flanges was machined down to 1 mm thickness to minimize sample holder interaction and attenuation of the neutron beam. The final sample holder assembly is shown in Fig. 6.

The sample was then exposed to the neutron beam at the Backscattering Silicon Spectrometer (BASIS) at the Spallation Neutron Source (SNS) located in Oak Ridge National Laboratory [9]. The incoming neutron beam of this time-of-flight (TOF) instrument has a bandwidth centered around 2082 μeV (0.6267 nm) (selected by application of the beam choppers). After the beam interacts with the sample, only the neutrons that have an energy of 2082 μeV scatter off of Si(1 1 1) crystals to be detected in a 2-D array of He-3 detectors. While offering a wide momentum-transfer range of 2 $nm^{-1} < Q < 20\ nm^{-1}$, energy transfers of up to ±200 μeV are simultaneously measured with 3 μeV (FWHM) resolution. Energy transfers are calculated as the difference between the incident neutron energy (determined from the overall time-of-flight before detection) and the fixed final energy of 2082 μeV selected by Si(1 1 1) reflections.

In this experiment, the instrument resolution function was collected at room temperature for each sample since hydrogen atoms are immobile on the time scale of the BASIS and scattering is almost purely elastic. The double-differential cross section corresponding to the scattering function was then obtained over the range of attainable momentum and energy transfers. Experimental data was collected for the two hydrides in the temperature range of 650–750 K with 25 K steps. The maximum temperature was limited by the integrity of the aluminum sample holder, while for temperatures lower than 650 K the limit is the extent of quasielastic broadening as it approaches the resolution of the instrument. This range is ideal since temperatures between these two limits span that of proposed LWR hydride fuel [5]. Data collection took place over a period of 6 h for each experimental temperature to achieve good statistics. The incoherent scattering function that upon its convolution with the resolution function corresponds to the measured intensities was extracted from the data using the

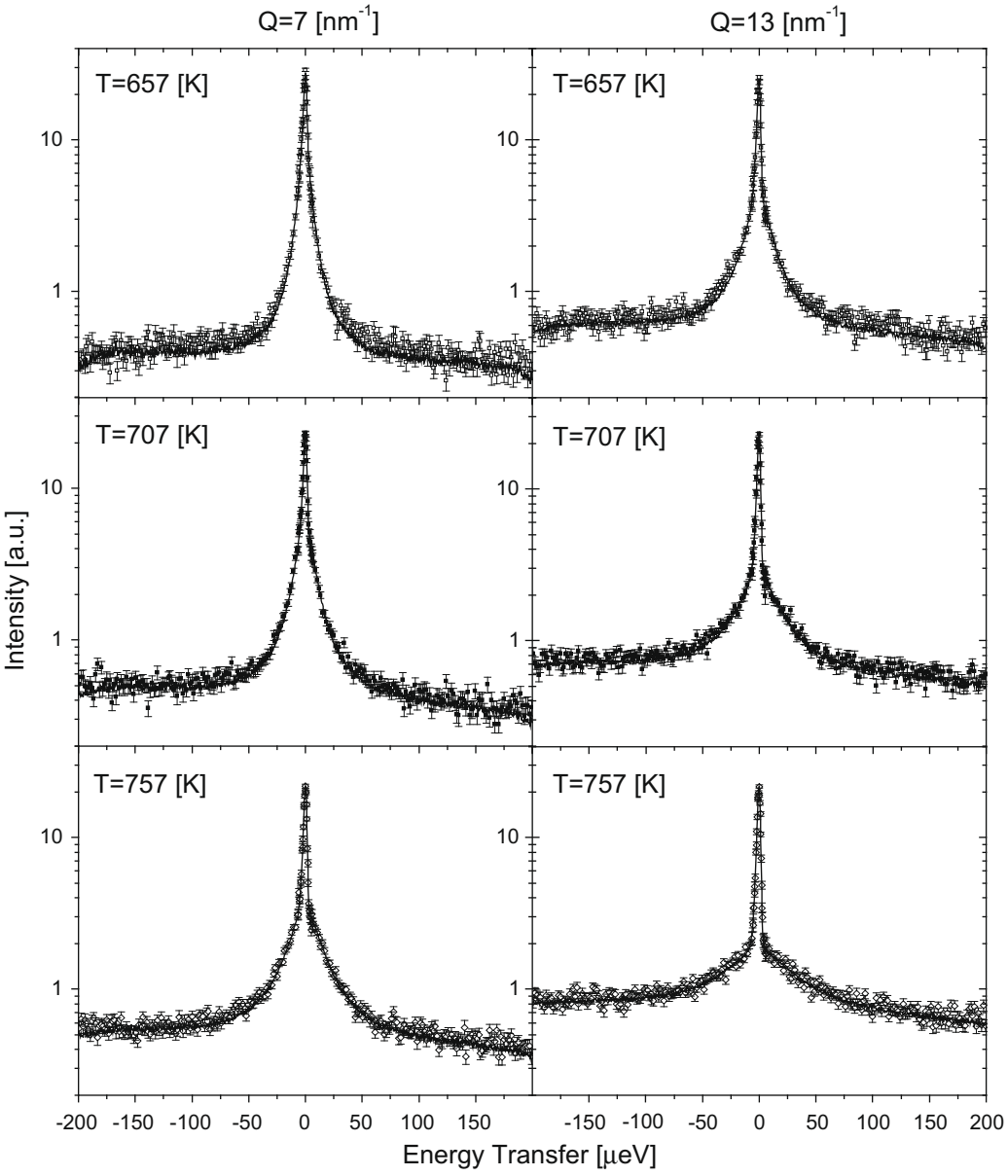

Fig. 7. Quasielastic spectra for $ThZr_2H_{5.6}$ at different temperatures and scattering momentum transfers.

DAVE software package [10]. No correction was made for multiple scattering at low angles since this effect is minimal for the thin samples.

5. Results

Quasielastic linewidth broadening of the spectra from $ThZr_2H_{5.6}$ is shown in Fig. 7. Even though the experiment has probed a relatively narrow temperature range, the change in the linewidth broadening is readily apparent. Broadening values were obtained using fits of the spectra with a Lorentzian quasielastic term, an elastic term, and a background term.

The isotropic Chudley–Elliott model [11] was applied in order to analyze the broadening of the incoherent scattering function (a Lorentzian function) at different temperatures. According to this model, the quasielastic linewidth (Λ) as a function of momentum transfer (Q) at each temperature is given by Eq. (1).

$$\Lambda(Q) = \frac{6\hbar D}{l^2}\left(1 - \frac{\sin(Ql)}{Ql}\right) \tag{1}$$

where $\hbar$, D, and l are Planck's constant, the diffusion coefficient, and the average jump distance, respectively. Eq. (1) is spatially averaged since a single-jump mechanism, representing an average of all possibilities, is assumed. Fitting the model to the experimental data in Fig. 8 shows excellent agreement between the two. Values for the diffusion coefficient and the jump distance were extracted from the data at each temperature through the fitting process. The Arrhenius dependence of the hydrogen diffusion coefficient and the atomic jump distance are shown in Figs. 9 and 10, respectively, and in Table 2.

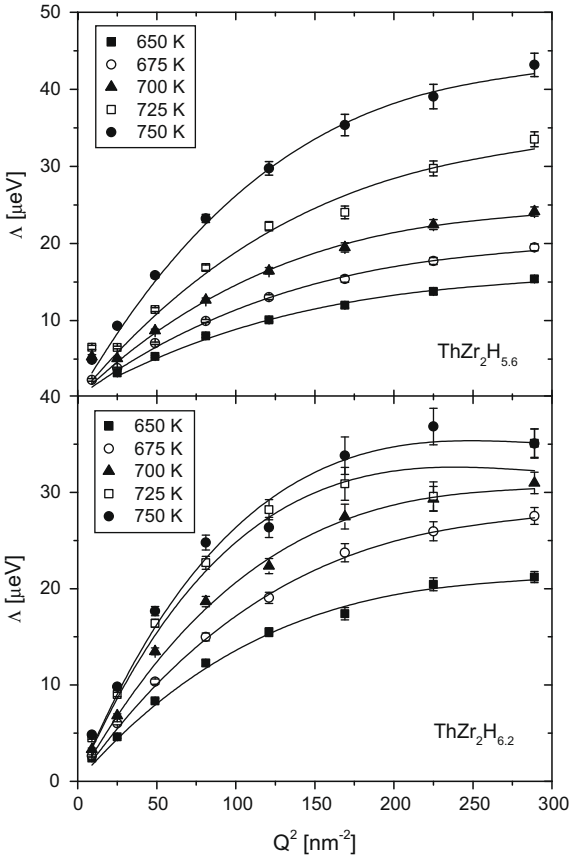

Fig. 8. Quasielastic linewidths (HWHM) as a function of Q^2 for $ThZr_2H_{5.6}$ and $ThZr_2H_{6.2}$.

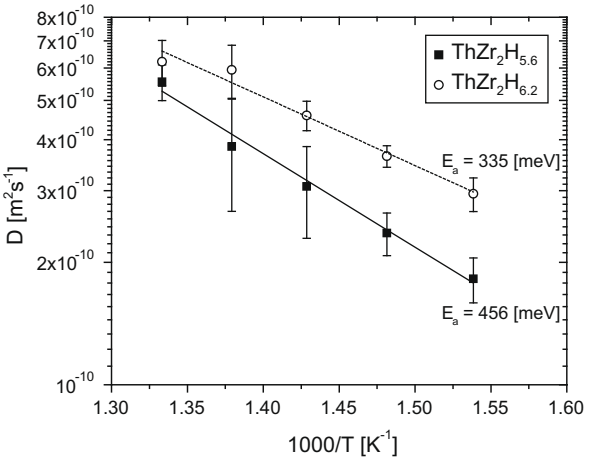

Fig. 9. Hydrogen diffusion coefficient in $ThZr_2H_{5.6}$ and $ThZr_2H_{6.2}$.

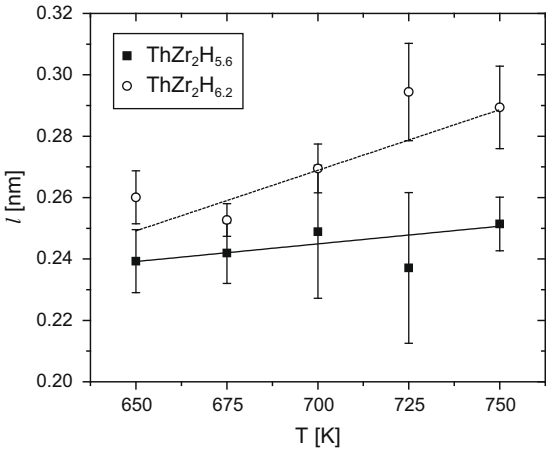

Fig. 10. Hydrogen atom jump distances in $ThZr_2H_{5.6}$ and $ThZr_2H_{6.2}$.

Table 2
Diffusion parameters and average jump lengths for hydrogen in thorium–zirconium hydride.

Material	D_o (10^{-7} m^2 s^{-1})	E_a (meV)	$\langle l \rangle$ (nm)
$ThZr_2H_{5.6}$	6.1 ± 4.8	460 ± 50	0.24 ± 0.01
$ThZr_2H_{6.2}$	1.2 ± 0.9	335 ± 50	0.27 ± 0.02

6. Discussion

6.1. Hydrogen atom jump

Although a large momentum-transfer range was probed, details regarding exact jump vectors could not be obtained due to the short H-atom jump distances. As discussed in Section 2, multiple jump scenarios exist based on the location of the H-atom inside the lattice. These possibilities are summarized in Table 3 along with the spacing between each of the two atomic sites. The distances are calculated from the structure and the lattice parameter of $ThZr_2H_{5.6}$ (0.912 nm). Based on a survey of a large number of stable hydrides, Switendick argues that the minimum H–H distance is no less than 0.21 nm [12]. Specifically for the $Fd\bar{3}m$ space group hydrides, Shoemaker and Shoemaker [13] suggest that no two adjacent tetrahedral hydrogen atom sites (i.e., sharing a common triangular face) can simultaneously accommodate hydrogen

Table 3
Routes and associated H-atom jump distances.

Initial position	End position	Coordination number of the jump	l (nm)
96(g)	32(e)	1	0.139
	96(g)	2	0.146
	96(g)	1	0.165
	96(g)	2	0.228
	32(e)	2	0.235
	96(g)	4	0.243
	32(e)	1	0.245
	96(g)	2	0.252
	96(g)	1	0.291
32(e)	96(g)	3	0.139
	96(g)	6	0.235
	96(g)	3	0.245
	32(e)	3	0.248

atoms. Neglecting distances less than 0.2 nm in Table 3, the average jump distances are in agreement with experimental values in Table 2.

The extent of error specified for each data point in Fig. 10 corresponds to one standard deviation in a normal distribution. Assuming that the true value of the jump distance is bound within this error window, the only possible jump path in Table 3 for the two highest temperature points in the $ThZr_2H_{6.2}$ sample is between two 96(g) sites with the spacing of 0.29 nm. This finding suggests a preferred path for hydrogen diffusion in this sample at high temperatures even though large momentum transfer regimes were not investigated. This change in the diffusion path at high temperatures is accompanied with a change in activation energy of diffusion that is associated with the specific jump vector. Consequently, this results in deviations from the simplified Arrhenius model fitted to the diffusion data in Fig. 9.

The average jump distance is the probability-weighted sum of all possible jump distances. The fitted lines to the data in Fig. 10 portray a direct relationship between average jump distance and the temperature. If the probability associated with each jump path is not a function of temperature, then the average jump distance is linearly proportional to the lattice parameter at each temperature. Therefore the coefficient of thermal expansion (CTE) could be estimated from the data in Fig. 10 using Eq. (2):

$$\alpha = \frac{d}{dT}\ln(l) \tag{2}$$

The values extracted for CTE from Fig. 10 are $3 \times 10^{-4}\,K^{-1}$ for $ThZr_2H_{5.6}$ and $1.5 \times 10^{-3}\,K^{-1}$ for $ThZr_2H_{6.2}$. These values observed based on increase of the average jump distance with temperature are orders of magnitude larger than what is typically detected from other hydrides ($\sim 2.5 \times 10^{-5}\,K^{-1}$ for zirconium hydride [14]). This result implies that the probability associated with each different jump is indeed a function of temperature where the probability for jump between two sites with larger spacing becomes more favorable with increasing temperature. This implication is consistent with the statements in the previous paragraph where deviations from simple Arrhenius behavior are expected.

6.2. Activation energy and pre-exponential term for hydrogen diffusion

The microscopic three-dimensional Einstein diffusion equation for interstitial hydrogen atoms can be expanded as follows:

$$D = \frac{1}{6} l^2 \eta \nu \exp\left(\frac{-E_a}{kT}\right) \tag{3}$$

where ν is the vibrational frequency and η is the product of the number of adjacent jump sites and the probability that the site is currently unoccupied by another hydrogen atom. Assuming that ν is equivalent for both hydrides, the difference in the observed pre-exponential factors can be explained by differing values of l and η. For large H/M ratios, hydrogen atoms have a slightly larger average jump distance. The probability of vacant adjacent interstitial site is one minus the fractional occupancy of available hydrogen sites. Although many interstitial sites for H atoms exist (see Section 2), the criterion set by Shoemaker indicates that the maximum H/M ratio is <7. If so, η for $ThZr_2H_{5.6}$ is 1.75 times larger in $ThZr_2H_{6.2}$. Thus, the larger pre-exponential factor for the lower stoichiometry hydride is expected.

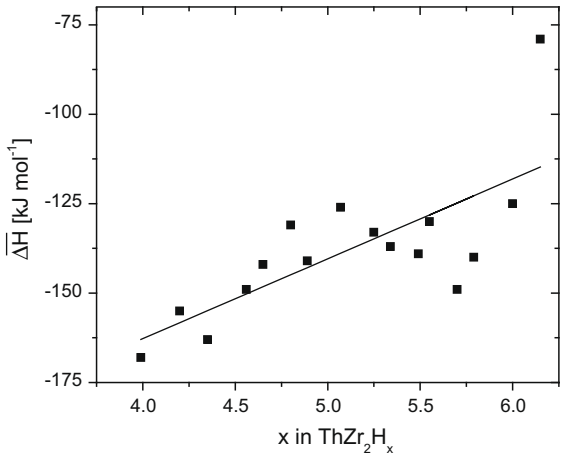

Fig. 11. Partial molar enthalpy of hydriding as a function of x in $ThZr_2H_x$ [1].

The dissimilar activation energies for hydrogen diffusion (E_a) in the two hydrides can be explained qualitatively by inspection of the pressure–temperature-composition equilibria [1]. The partial molar enthalpy of hydriding at different hydrogen-to-metal ratios is shown in Fig. 11. A rather complex relationship between the partial molar enthalpy of hydriding and hydrogen concentration in the hydride exists, implying that the fractional occupancy of the possible hydrogen sites and the bonding strength at each site are complex functions of hydrogen concentration. The fractional occupancy of the 96g and 32e sites has been measured in ref [6] and indeed shows a nonlinear variation with hydrogen concentration at room temperature. In the meantime it is possible to discern a decreasing trend in $\overline{\Delta H}$ (absolute value) with increasing H/M ratio in Fig. 11. This trend suggests a reduction in the strength of the average hydrogen–metal bond as the hydrogen content of the hydride increases. This implies that H atoms in the lower stoichiometry hydride are more tightly bonded and require larger activation energies to overcome the jump barrier than in the higher hydride. This implication is in agreement with what is observed experimentally.

7. Conclusions

Quantification of hydrogen diffusivity in Th–Zr hydrides is of great interest to design and optimize hydride fuel fabrication processes and to model fuel behavior under steady state and transient-power conditions. In order to measure interstitial hydrogen diffusion, quasielastic broadening of the incoherent-neutron-scattering signal from ternary thorium–zirconium hydrides has been determined over the temperature range 650–750 K. This temperature range is typical of hydride nuclear fuel under steady state reactor operation. The measurement was done over a wide range of energy and momentum transfers, simultaneously and rapidly, using the time-of-flight backscattering spectrometer (BASIS) at the Spallation Neutron Source at

ORNL. The isotropic Chudley–Elliott diffusion model accurately predicts the measured variation of the quasielastic Lorentzian linewidth broadening as a function of momentum transfer. Using this data the pre-exponential term and the activation energy of hydrogen diffusion in two Th–Zr hydrides could be quantified applying a simplified Arrhenius model.

Although the hydrogen jump distance is small and the probed momentum-transfer range (corresponding to distance in reciprocal space) was limited, the spatially-averaged jump distances of hydrogen atoms extracted from the isotropic Chudley–Elliott model are in agreement with the structural information. The difference in the average activation energy for hydrogen atom jump at different hydrogen concentrations is also coherent with the available thermodynamic information. Meanwhile, recognizing the complex structure of Th–Zr hydrides where multiple hydrogen atom sites and jump paths with different bonding strengths and activation energies are present, deviations from the simplified Arrhenius behavior is expected over larger temperature ranges.

Acknowledgements

The efforts at Ames Laboratory's Materials Preparation Center and Oak Ridge National Laboratory's Spallation Neutron Source were sponsored by the Scientific User Facilities Division, Office of Basic Energy Sciences, US Department of Energy. The aid and valuable technical insight of Dr. Wigbert Siekhaus at Lawrence Livermore National Laboratory is also gratefully acknowledged.

References

[1] W. Bartscher, J. Rebizant, J.M. Haschke, J. Less-Common Met. 136 (1988) 385.
[2] K.A. Terrani, G.W. Chintaka Silva, C.B. Yeamans, M. Balooch, D.R. Olander, J. Nucl. Mater. 392 (2009) 151.
[3] T. Yamamoto, H. Suwarno, H. Kayano, M. Yamawaki, J. Nucl. Mater. 247 (1997) 339.
[4] D.R. Olander, Fundamental Aspects of Nuclear Reactor Fuel Elements, Natl. Tech. Info. Services. Document No. 26711, 1976, p. 77.
[5] K.A. Terrani, J.E. Seifried, D.R. Olander, J. Nucl. Mater. 392 (2009) 192.
[6] W. Bartscher, J. Rebizant, A. Boeuf, R. Caciuffo, F. Rustichelli, J.M. Fournier, W.F. Kuhs, J. Less-Common Met. 121 (1986) 455.
[7] H. Okamoto, Th–Zr (Thorium–Zirconium), in: T.B. Massalski (Ed.), Binary Alloy Phase Diagrams, vol. 3, second ed. 1990, p. 3488.
[8] R. Hempelmann, Quasielastic Neutron Scattering and Solid State Diffusion, Oxford University Press Inc., 2000.
[9] E. Mamontov, M. Zamponi, S. Hammons, W.S. Keener, M. Hagen, K.W. Herwig, Neutron News 19 (3) (2008) 22.
[10] Data Analysis and Visualization Environment, NIST Center for Neutron Research. <http://www.ncnr.nist.gov/dave>.
[11] C.T. Chudley, R.J. Elliott, Proc. Phys. Soc. 77 (1961) 353.
[12] A.C. Switendick, Z. Phys. Chem. Neue Folge 117 (1979) 89.
[13] D.P. Shoemaker, C.B. Shoemaker, J. Less-Common Met. 68 (1979) 43.
[14] S. Yamanaka, K. Yoshioka, M. Uno, M. Katsura, H. Anada, T. Matsuda, S. Kobayashi, J. Alloys Compd. 293–295 (1999) 23.